Metabolic homeostasis in chronic helminth infection is sustained by organ-specific metabolic rewiring

Kokova, D.; Verhoeven, A.; Perina, E.A.; Ivanov, V.V.; Heijink, M.; Yazdanbakhsh, M.; Mayboroda, O.A.

ACS Infectious Diseases

pubs.acs.org/journal/aidcbc

Article

Metabolic Homeostasis in Chronic Helminth Infection Is Sustained by Organ-Specific Metabolic Rewiring

Daria Kokova, Aswin Verhoeven, Ekaterina A. Perina, Vladimir V. Ivanov, Marieke Heijink, Maria Yazdanbakhsh, and Oleg A. Mayboroda*

Cite This: *ACS Infect. Dis.* 2021, 7, 906–916

Read Online

ACCESS | Metrics & More | Article Recommendations | Supporting Information

ABSTRACT: Opisthorchiasis, is a hepatobiliary disease caused by flukes of the trematode family *Opisthorchiidae*. A chronic form of the disease implies a prolonged coexistence of a host and the parasite. The pathological changes inflicted by the worm to the host's hepatobiliary system are well documented. Yet, the response to the infection also triggers a deep remodeling of the host systemic metabolism reaching a new homeostasis and affecting the organs beyond the worm location. Understanding the metabolic alternation in chronic opisthorchiasis, could help us to pinpoint pathways that underlie infection opening possibilities for the development of more selective treatment strategies. Here, with this report we apply an integrative, multicompartment metabolomics analysis, using multiple biofluids, stool samples and tissue extracts to describe metabolic changes in *Opisthorchis felineus* infected animals at the chronic stage. We show that the shift in lipid metabolism in the serum, a depletion of the amino acids pool, an alteration of the ketogenic pathways in the jejunum and a suppressed metabolic activity of the spleen are the key features of the metabolic host adaptation at the chronic stage of *O. felineus* infection. We describe this combination of the metabolic changes as a "metabolically mediated immunosuppressive status of organism" which develops during a chronic infection. This status in combination with other factors (e.g., parasite-derived immunomodulators) might increase risk of infection-related malignancy.

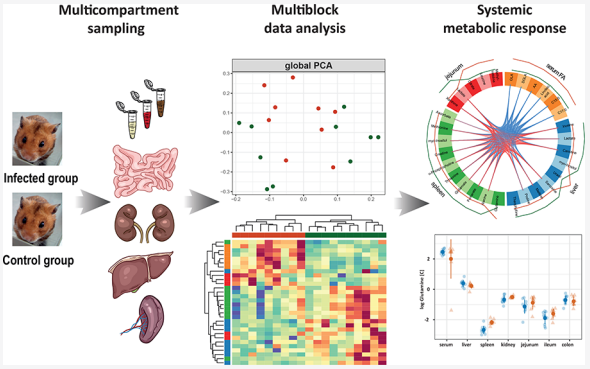

KEYWORDS: *metabolomics, NMR spectroscopy, opisthorchiasis, chronic infection, metabolic remodeling*

Opisthorchiasis a hepatobiliary disease is caused by flukes of the trematode family *Opisthorchiidae*: *Opisthorchis felineus*, *Opisthorchis viverrini*, and *Clonorchis sinensis*. Together, these three species affect more than 45 million people in endemic regions.[1,2] The clinical manifestations of acute opisthorchiasis are nonspecific, and its chronic form usually appears asymptomatic.[3,4] Yet, at the chronic stage of infection, there is a progressive accumulation of pathological changes in the host due to egg-induced fibrosis and the local damage inflicted to the biliary epithelium by the worms. Moreover, a long-term coexistence with a parasite leads to a remodeling of the host systemic metabolism. How and at what cost this new homeostasis is sustained is still poorly understood, but a current theoretical framework[5] implies that metabolic shift has a profound influence on the host immune status and eventually affects organs that are not directly involved in the immune response. Understanding the metabolic alteration in opisthorchiasis could help us understand the pathways that underlie infection and disease progression that might be targets of therapeutics.

Metabolomics offers a method for exploring systemic metabolism. Today, metabolomics of helminth infections is an area of active research. It has been shown that the metabolic response of the host usually leads to changes in the pattern of amino acids in the body fluids, remodeling of the lipid metabolism, and changes in composition of microbiota-related metabolites.[6] Yet, while metabolic responses to helminth infections in animal models are rather strong and easily detectable, field studies with human participants have shown that these infections are not one of the strongest influences on the metabolic composition of body fluids. The traditional confounding factors such as age, gender, BMI, and lifestyle mask the infection related metabolic adaptations.[7] Of course, one of the main differences between field studies and animal experiments is the degree of control over the sources of the unwanted variance. Another difference is that animal studies often report only the effects observed at an early stage of the

Received: January 19, 2021
Published: March 25, 2021

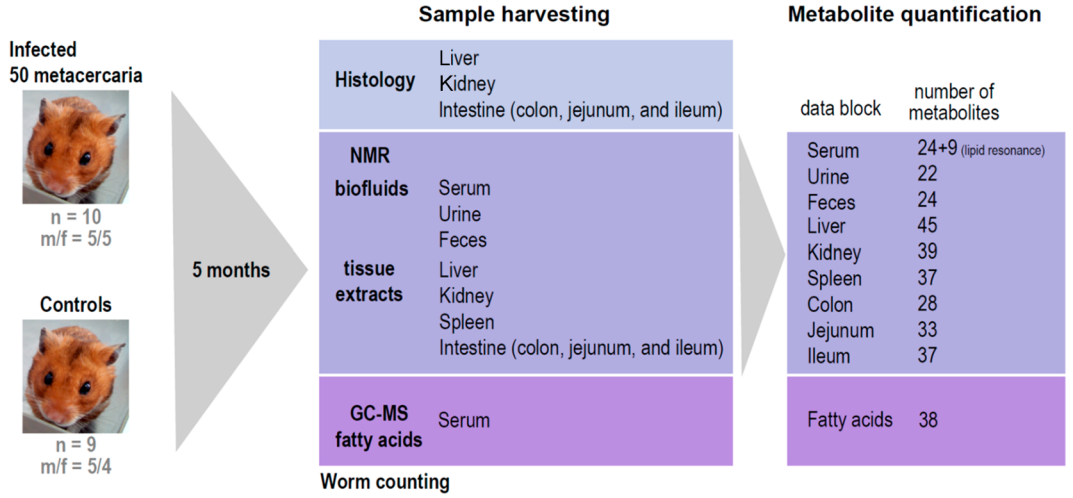

Figure 1. Study design. Twenty golden Syrian hamsters (*Mesocricetus auratus*) of both genders were divided into two groups. Ten animals (five males and five females) were infected orally with 50 *O. felineus* metacercariae (Infected group). The remaining ten hamsters (five males and five females) were kept as a control group. During the experiment one female animal in the infected group died. Serum, urine, feces, liver, kidney, spleen, and intestine samples were collected in the 20th week postinfection from the animals of both groups for NMR, GC-MS and histological analysis.

infection, while in a "real life" situation it is the chronic stages of infection that we are likely to encounter.

Recently, using an experimental infection system with the liver fluke *O. felineus*, we have shown that in urine and blood the metabolic response stabilizes after the 12th week of infection when hardly any statistically significant changes can be found between infected and uninfected animals.[8,9] Here, to emulate the chronic stage of infection, data are generated over 20 weeks postinfection. Moreover, the systemic changes in the metabolism are not expected to be limited to serum or urine but could affect multiple organs and functional systems of an organism. Therefore, for the first time, a multicompartment approach was used for a detailed description of the metabolic phenotype of a chronic helminth infection, beyond the conventionally used biofluids (blood, urine). The choice of compartments was guided by the current views on parasite biology and published studies on the morbidities associated with opisthorchiasis. To this end, we analyzed, in addition to serum, urine, and stool samples, the liver, where the flukes reside, the three segments of intestine, jejunum, ileum, and colon, where the eggs of the flukes are usually passed and can get trapped in granulomas, as well as the spleen, the largest part of the lymphatic system involved in the immune response of a host to a parasite infection.[10,11] It has been shown that opisthorchiasis leads to nephropathy; thus, the kidney, one of the key metabolic organs, was also included in our analysis.[12,13] Finally, not only have we looked at the metabolomics using NMR but we have also used quantitative gas chromatography–mass spectrometric profiling of fatty acids in peripheral blood, considering the role that lipid metabolism plays in a host response to an infection. Every compartment delivers an independent set of the data, which we refer to as "data blocks". In total, 11 data blocks corresponding to each of the sample types (serum, urine, feces, liver, kidney, spleen, colon, jejunum, ileum, serum lipids, and serum fatty acids) were generated and analyzed (Figure 1).

Thus, with this report, we for the first time perform an analysis that integrates metabolomics data from multiple biofluids and tissue extracts to describe metabolic changes in *O. felineus* infected animals at the chronic stage. We show that a shift in the lipid metabolism in the serum and metabolism changes in the spleen are the key features of the metabolic host adaptation at the chronic stage of *O. felineus* infection.

RESULTS

Outline of the Experiment, Basic Animal Characteristics, Histology, and Metabolite Quantification. Figure 1 summarizes our experimental design: an observational study with two (infected vs noninfected) equally sized experimental groups. One animal died before the end of the experiment, and thus, our final sample consisted of 19 animals: 10 controls (5 females and 5 males) and 9 infected animals (4 females and 5 males). At the end of the experiment, the median body weight of the animals in the control and infected group was 133.85 and 118.20 g, respectively, with no statistically significant difference. However, a gender specific comparison shows that the body weight of the infected female animals is significantly lower than that of noninfected ones (p-value = 0.04). Similarly, the liver weight shows no significant difference between the infected and noninfected groups, while a gender specific comparison shows an increase in the liver weight for the infected male animals (p-value < 0.0001) (Figure S1).

To obtain a representative overview of the metabolic differences between the infected and noninfected animals at 20 weeks postinfection, we collected the main biofluids (blood and urine), feces, the main metabolic organs (liver and kidney), three segments of the digestive tract (colon, ileum and jejunum), and the spleen. The histological analysis shows no difference between the segments of the digestive tract or the kidney of the infected and uninfected groups. The liver samples of *O. felineus* infected animals had areas of inflammatory cell infiltration occurring around the bile ducts. The histological analysis of the liver samples of the control group showed no evidence of pathological changes in the liver or the bile ducts (Figure S2).

For metabolomics analysis, we took a quantitative targeted approach. Using the Chenomx NMR suite, we quantified 22 metabolites in urine, 45 in liver, 39 in kidney, 37 in spleen and ileum, 33 in jejunum, 28 in colon samples, 24 in feces, and 24 in the serum samples. Moreover, for serum, 9 resonances

https://doi.org/10.1021/acsinfecdis.1c00026
ACS Infect. Dis. 2021, 7, 906−916

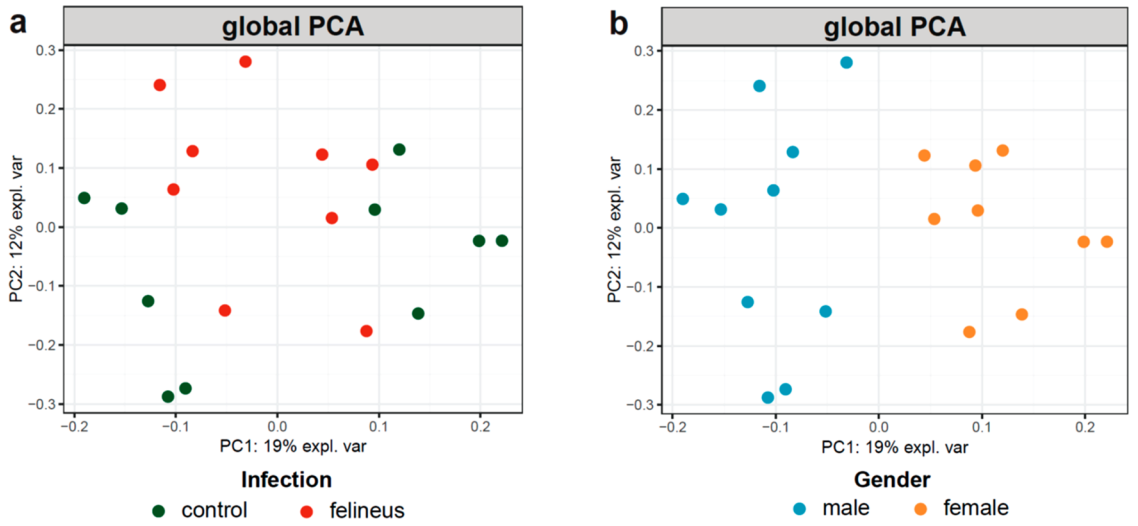

Figure 2. Scores plot the first two principal components (PCs) of the global PCA model built on all data sets: (a) colored by the infection status; (b) colored by gender of an animal. The model shows that not the infection but gender is the main source of variance in the combined model.

corresponding to the different chemical groups of the molecules in the serum lipoproteins were integrated (Supporting Information Excel file data) and 38 short-, long-, and very-long-chain fatty acids in serum samples were quantified using mass spectrometry. Only alanine and lactate were detected in all studied samples; tyrosine, valine, choline, phenylalanine, isoleucine, and leucine were found almost in all samples apart from urine. Creatine, glutamine, glutamate, uracil, fumarate, and glucose were quantified in all tissue samples. Figure S3 summarizes the quantified metabolites across the samples.

Multiblock Analysis and Selection of the Relevant Data Blocks. Figure 2 shows a score plot of the global PCA model built on all 11 data blocks using an unsupervised multiple kernel method.[14] The method enables an integrated overview of the major trends in the data. The model required five principal components (PCs) to explain 56% of the variance with 31% covered by the first two components. The score plot of the model shows that not the infection (Figure 2a) but gender (Figure 2b) is the main source of variance in the combined model. The gender-related clustering is associated with the strongest component of the combined model which explains 19% of the total variance (Figure 2). To estimate the relative contribution of each individual block to the variance associated with infection, we applied an unsupervised multiblock modeling approach with correction for the gender effect. A practical realization of such analysis is the Multi-Omics Factor Analysis (MOFA) algorithm.[15] MOFA can be viewed as a generalization of PCA for multiblock problems, which obtains a set of latent factors capturing the major variation across multiple data sets. Figure 3 summaries the MOFA model built on 11 available blocks of data. The model converged to 10 factors, which cumulatively explain 77% of variation in the colon samples, 56% in the ileum, 56% in the jejunum, 70% in the liver, 77% in the spleen, 50% in the kidney, 71% in the urine samples, 65% in the stool, 69% in the serum, 70% in serum fatty acids, and only 8% in the lipoprotein block (Figure 3a). An overview of all factors (Figures S4 and 3b) shows that the latent factor 6 is aligned with the status of infection. Figure 3c shows the contribution of the individual data blocks to latent factor 6. It is evident that four blocks, namely, the serum fatty acids (15% of the variance), jejunum (13%), liver (12%), and spleen (12%), have strongest influence on the factor. Figures S5−S8 show the heat maps for the four selected blocks visualizing the weights of the individual metabolites on latent factor 6. However, even though the changes between the infected and noninfected animals can be identified visually, a selection of the most relevant metabolites which could compose an "infection signature" requires a regression-based strategy.

Metabolic Signature of Chronic Opisthorchiasis. Figure 4a shows the distribution of the individual samples along the first two components of the multiblock regression model. All data sets show clear clustering of two sample groups on the first component (covers 41.3% of variance in spleen data, 31.3% in liver, 27.8% in serum fatty acids, and 17.6% in jejunum). Figure 4b presents the variables in a clustered image map (Figure 4b) based on the Euclidean distance and complete linkage. It displays an unsupervised clustering between selected metabolites of the spleen, liver, jejunum, and serum fatty acids and the animals. Figure 4b presents all significantly increased serum fatty acids in the infected animals; concentrations of inosine, lactate, myo-inositol, proline, sarcosine, theophylline, maltose, and carnitine are suppressed in the infected group, while liver uracil is increased; levels of methyl-histidine, leucine, and citrate in the jejunum of the *O. felineus* group are increased, while jejunum lactate and xanthine are decreased; and in the spleen, the level of glutamine is increased in the presence of opisthorchiasis, when most metabolites are suppressed: ascorbate, alanine, myo-inositol, methionine, creatine, glutamate, fumarate, *o*-phosphocholine, and threonine. Figure 5 shows the correlation between the selected variables of the different blocks (correlation cutoff | 0.7|). Remarkably, all serum fatty acids show negative correlations with the metabolites of the tissues. The liver metabolites, namely, inosine, lactate, carnitine, sarcosine, proline, and maltose, positively correlate with the spleen and jejunum. With exception of glutamine, all spleen metabolites show positive correlations with the metabolites of liver and jejunum and a negative one with the fatty acids; yet ascorbate correlates only with jejunum xanthine and serum DGLA. Of the jejunum metabolites, only lactate and xanthine show a correlation with other data blocks.

To assess the performance of our model, we applied 5-fold cross validation. Table S1 summarizes the cross-validated AUC

https://doi.org/10.1021/acsinfecdis.1c00026
ACS Infect. Dis. 2021, 7, 906−916

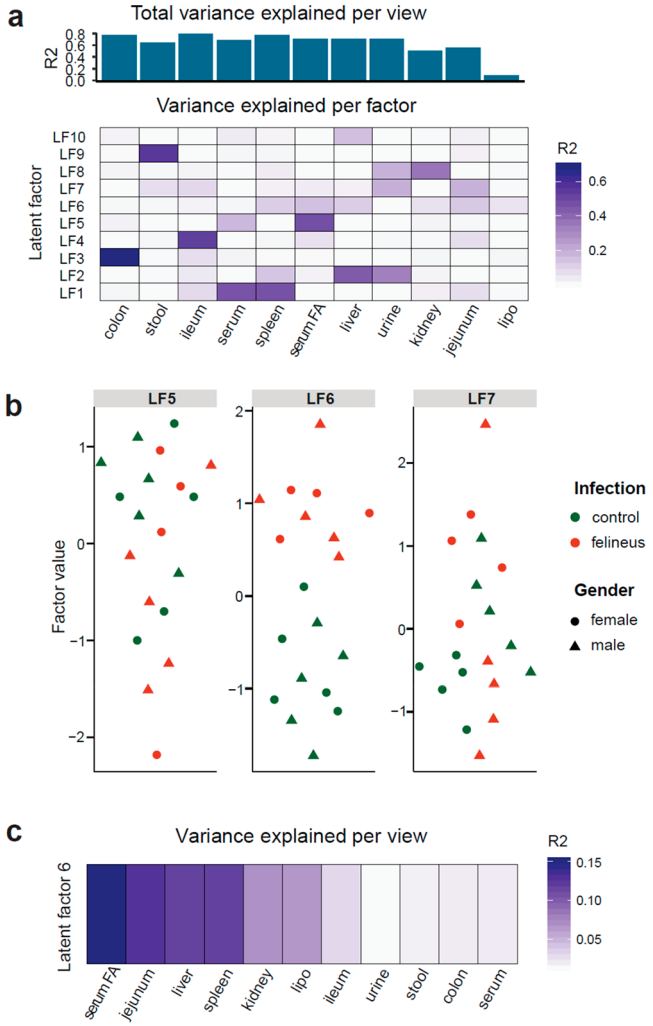

Figure 3. Multi-Omics Factor Analysis (MOFA) modeling. The model is built on the 11 available blocks of data. (a) Cumulative proportion of total variance (R2) per block of the data and variance explained per factor in each data block. (b) Swam plots showing the sample clustering along the factors values for the latent factors 5, 6, and 7; color shows infection status, and shape shows gender. (c) Representation of decomposition of variance (R2) in the latent factor 6 in each data block (view).

values and their respective *p*-values for each block. Finally, we used an unsupervised clustering approach to test the selected subset of metabolites. Figure S9 shows the results of a PCA of the K-means clusters built on the selected variables; the samples are clustered according to the infection status, which implies that the samples within the clusters have similar metabolic characteristics.

Pathway Enrichment Analysis on the Metabolic Signature of Chronic *O. felineus* Infection. To get insight into the metabolic networks which could be associated with the infection, we used the MetExplore environment. MetExplore can map the selected subsets of metabolites into the pathways using organism-specific databases. To this end, we used the following subset of spleen metabolites for the mapping: ascorbate, methionine, myo-inositol, creatine, *o*-phosphocholine, threonine, fumarate, alanine, and glutamate. Seven significant pathways involving 30 reactions (Table 1) were chosen based on the Bonferroni-corrected *p*-values. All metabolites, except *o*-phosphocholine, were mapped into the subnetworks (Figure S10). The mapping of the liver metabolites did not result in any significantly enriched pathways (*p*-value $\geq$ 0.05). For the jejunum, only leucine and citrate were significantly associated with 2-oxocarboxylic acid metabolism. Thus, the limited number of metabolites that the analysis yields certainly restricts the possibilities for interpretation. Yet, the spleen data clearly points toward a dysregulation in the glutathione, glutamate, and alanine balance.

Systemic Balance of Glutamine. It has been shown that an active infection process increases the catabolism of glutamine by the immune cells and as such changes the balance of glutamine and therefore the glutamine/glutamate and the glutamine/alanine ratios.[16] Figure 6 shows a comparative overview of the glutamine balance for serum and all analyzed tissue samples. In agreement with existing data on the glutamine distribution, its concentration in serum is higher than that in the tissues, but there is no significant difference between serum concentrations of glutamine of the infected and noninfected animals. The glutamine/glutamate ratio is significantly lower in the liver of the infected animals (*p*-value = 0.02). The most consistent changes are observed in the spleen: the concentration of glutamine (*p*-value = 0.0007) and corresponding glutamine/glutamate (*p*-value <0.00001) and glutamine/alanine (*p*-value < 0.00001) ratios are higher in the spleen of the infected animals.

DISCUSSION

Metabolic phenotyping of pathological conditions is often restricted to the most accessible types of biological samples such as urine, serum, and feces. Yet, the systemic changes in the metabolism are not limited to the serum or urine but affect multiple organs and functional systems of an organism. Thus, aiming for an extended study of the metabolic phenotype of chronic O. *felineus* infection we analyzed the samples from the most relevant compartments in the body. We have generated 11 data blocks, the blocks corresponding to the compartments analyzed. A set of four blocks, liver, spleen, jejunum, and serum fatty acids, were needed to explain the variance of the data related to chronic infection with *O. felineus* (Figure 3). Thus, we can conclude that with the exception of the serum fatty acids the metabolic composition of the biofluids at the chronic stage of the infection remains rather similar to the composition in noninfected animals. This observation is in an agreement both with reports on human material[7] and our recent publication on an animal model.[8,9] Indeed, field studies on human body fluids show that the traditional confounding factors such as age, gender, BMI, and lifestyle affect the metabolic composition more strongly than the infection and simply override the effect of the infection. In our animal model report, we have shown that infection-related metabolomic changes in urine are the most pronounced from the 4th week up to the 12th week postinfection. At later time points, no significant differences between the infected and control animals were detected.[8] The same applies to serum metabolites and serum lipoprotein clusters: the statistically significant changes in amino acids and lipid clusters were observed in the first weeks after infection.[9] Only few metabolites remained marginally different beyond the 10th week of infection. Thus, the current results and our previous reports show that after the initial state of "metabolic stress"[8,9] the organism reaches a state of metabolic homeostasis. This homeostasis, however, is

https://doi.org/10.1021/acsinfecdis.1c00026
ACS Infect. Dis. 2021, 7, 906−916

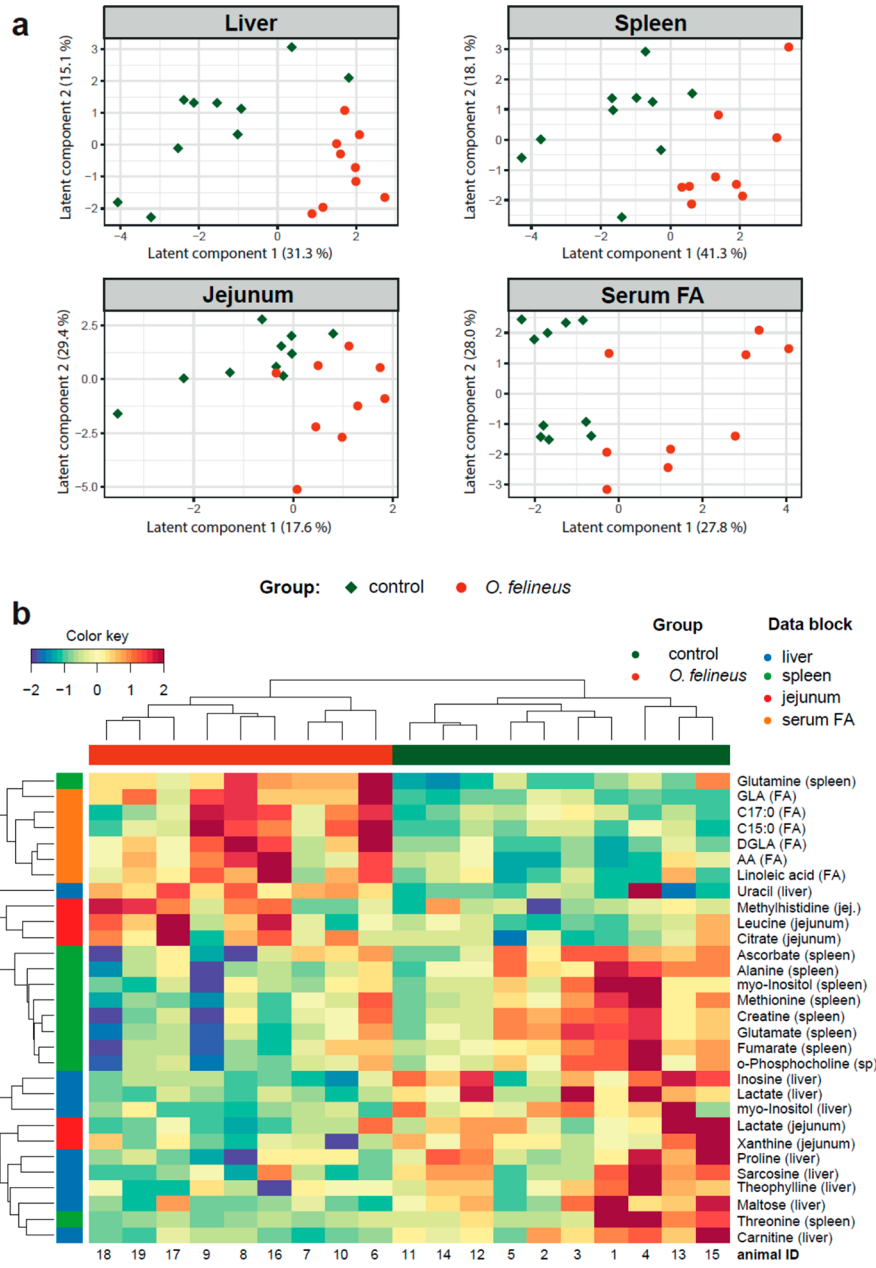

Figure 4. DIABLO modeling. (a) Scores plots of each data blocks based on the first and the second components from the DIABLO model. (b) Heat map built on the subset of the variables selected by a DIABLO model; the columns present the observations, and the rows present the discriminating metabolites.

sustained by a shift in the systemic lipid metabolism and local, organ-specific metabolic adaptive changes.

Indeed, here we indicate that the circulating serum fatty acids, liver, spleen, and jejunum show the strongest contribution to the systemic metabolic changes associated with chronic opisthorchiasis. While our analysis does not exclude the possibility that other body compartments may contribute, the ones we identified here appear essential for the description of the metabolic changes triggered by chronic *O. felineus* infection. Our results show that the "integrated metabolic signature" of chronic opisthorchiasis consists of 30 structures associated with lipid, amino acid, and energy metabolism. Moreover, six serum fatty acids, glutamine in the spleen, uracil in the liver, and methyl-histidine, leucine, and citrate in the jejunum form a cluster of compounds that are increased in the chronically infected animals. The remaining 22 metabolites are depleted in the chronically infected group. Thus, the most important metabolic features of the chronic *O. felineus* infection are the increase in the circulating serum fatty acids, depletion of the amino acids pool in liver, spleen and jejunum. We believe that the given pattern points toward a specific type of systemic metabolic adaptation.

Indeed, a subset of free fatty acids contributing to the infection signature contains two odd-chain fatty acids (pentadecanoic and heptadecanoic acids) and a group of functionally linked structures, namely LA, GLA, DGLA and AA. All those structures were reported as having a reverse association with the risk of type 2 diabetes.[17−19] Moreover, all mentioned fatty acids are either essential or conditionally essential which implies their dietary origin or, as the recent

https://doi.org/10.1021/acsinfecdis.1c00026
ACS Infect. Dis. 2021, 7, 906−916

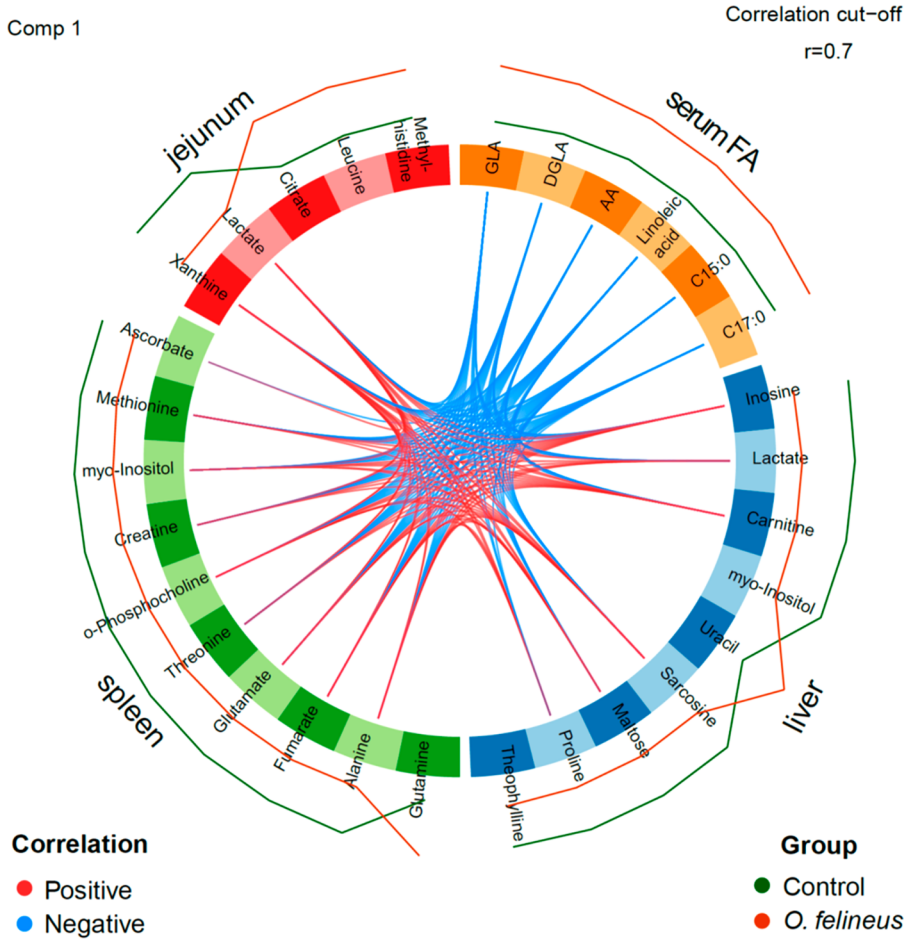

Figure 5. Plot shows the correlations (cutoff is 0.7) between variables of different blocks. All serum fatty acids show negative correlations with the metabolites of the tissues. With exception of glutamine, all spleen metabolites show positive correlations with liver and jejunum and negative one with the fatty acids. Of the jejunum metabolites, only lactate and xanthine show correlation with other data blocks.

Table 1. Results of the Pathway Enrichment Analysis Run on the Metabolites Selected by DIABLO Multiblock Modeling

significant pathway	KEGG identifier	number of metabolites	corrected *p*-value
spleen			
biosynthesis of amino acids	cge01230	6	2.4×10^{-5}
aminoacyl-tRNA biosynthesis	cge00970	5	1.7×10^{-4}
alanine, aspartate, and glutamate metabolism	cge00250	4	7.9×10^{-4}
arginine and proline metabolism	cge00330	4	5.9×10^{-3}
glutamine and glutamate metabolism	cge00471	2	0.017
nitrogen metabolism	cge00910	2	0.023
ascorbate and aldarate metabolism	cge00053	2	0.049
jejunum			
2-oxocarboxylic acid	cge01210	2	0.02

report on C15:0 and C17:0 fatty acids shows, their production by gut microbiota.[20,21] Therefore, the characterization of the microbiome at the chronic stage of opisthorchiasis should shed light on this. In turn, this makes it possible to suggest the involvement of microbiota in the regulation of metabolic homeostasis during the chronic infection. Furthermore, a recently published meta-analysis of metabolic markers of prediabetic and diabetic subjects shows that the increased concentrations of the BCAAs, aromatic amino acids, alanine, and lactate and the glutamine/glutamate ratio in the blood are characteristic for these conditions.[22] In our report on the time-resolved metabolomics of serum during *O. felineus* infection, we observed a strong decrease of the BCAAs during the first weeks of infection.[9] Although the depletion of the circulating BCCAs stabilizes around the 10th week, their levels remain lower than those for the controls during the entire 22 weeks of the experiment.[9] In the current report, the concentration of alanine in the infected animals was lower not only in the liver and spleen, the organs which contribute to the infection signature, but also in serum (Figure 6). Considering the data on the negative association between helminth infections and the risk of metabolic syndrome,[23] one might be tempted to focus on the similarities between the changes in the systemic metabolism triggered by the chronic *O. felineus* infection and "protective" metabolic patterns. Yet, the chronic infection with *O. felineus* increases the risk of liver pathologies and even cancer;[24] thus, we believe that the prolonged changes in the utilization of the main metabolic fuel components and the local depletion of the amino acids pool leads gradually to a physiological condition which can be labeled as a "metabolically driven immunosuppresion". For instance, we show that the metabolic activity of the spleen is suppressed in the infected animals; our data show the increased concentrations

https://doi.org/10.1021/acsinfecdis.1c00026
ACS Infect. Dis. 2021, 7, 906−916

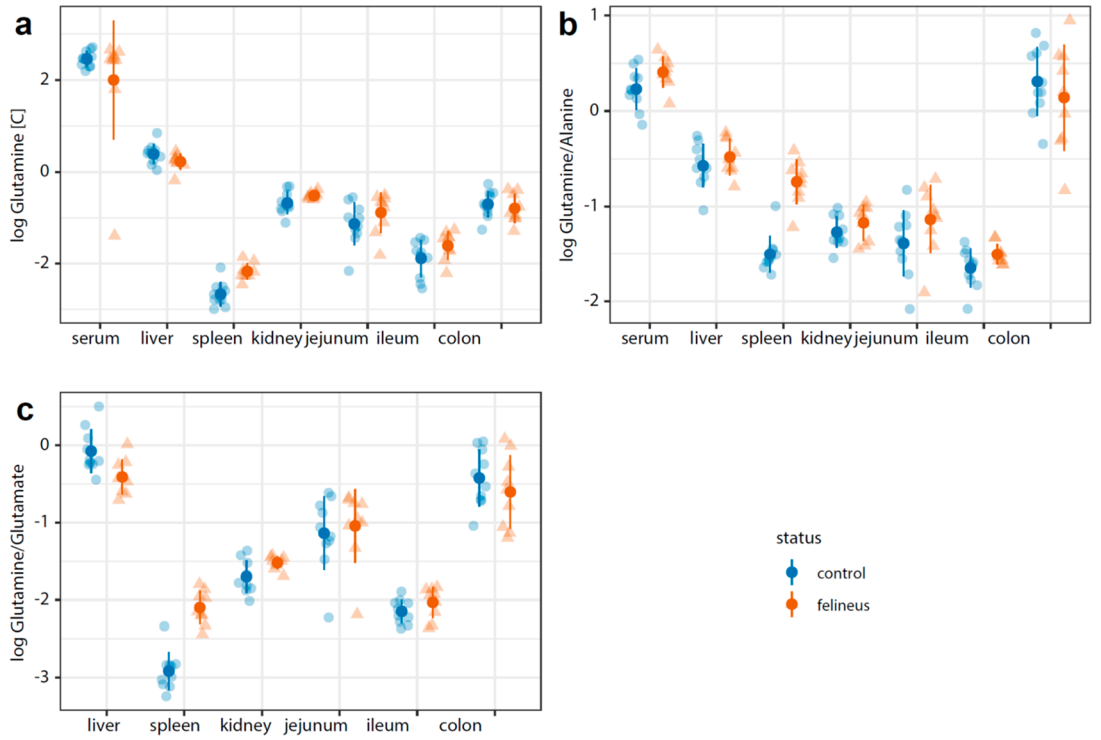

Figure 6. Overview of glutamine balance. (a) Glutamine, (b) glutamine/alanine ratio, and (c) glutamine/glutamate ratio. (a) The glutamine concentration in serum was higher than that in the tissues, but there is no significant difference of serum glutamine concentrations between the infected and noninfected animals. The most consistent changes are observed in the spleen (p-value = 0.0007). (b) The glutamine/alanine ratio is higher in the spleen of the infected animals (p-value < 0.00001). (c) The glutamine/glutamate ratio is significantly lower in the liver tissue (p-value = 0.02) and higher in spleen tissue (p-value < 0.00001) for the infected animals.

of glutamine/glutamate and glutamine/alanine ratios in the spleen of the infected animals. This, in turn, implies a reduced conversion of glutamine to glutamate by glutaminase. The glutamine/glutamate ratio is often used for a rough assessment of the cell proliferation activity: a high ratio indicates a reduced consumption of glutamine and consequently lower proliferation rates within the organ.[25] It is worth mentioning that in liver the glutamine/glutamate ratio is shifted in the opposite direction, thus suggesting a higher metabolic activity of the liver of the infected animals. This is in agreement with the response of the liver to the presence of the parasite, the adaptations to the mechanical damage of the biliary system, and the processes controlling the inflammation, eosinophilia, and periductal fibrosis.[26] All those factors are probably responsible for the increased weight of the organ in the infected animals (Figure S1). Finally, the pathway enrichment analysis suggests an alteration in the keto-acids pathways (2-oxocarboxylic acids metabolism) in the jejunum, which is in agreement with the reported increased concentration of leucine (Figure S11). Leucine is a strictly ketogenic amino acid, which implies that it is converted to fat rather than glucose. Moreover, an active catabolism of leucine is essential for the regulation of intestinal immune function[27] and the regulation of the entire mTOR signaling system.[28] Thus, even though our ability to draw firm mechanistic insights is restricted by the limited number of metabolites that change upon chronic opisthorchiasis, they do indicate a local depletion of the amino acids pool, an alteration of the ketogenic pathways in the jejunum, and last but not least a suppressed metabolic activity of the spleen. We can tentatively describe this combination of metabolic changes a "metabolically mediated immunosuppressive status of the organism" which develops during a chronic infection. This status in combination with other factors (e.g., parasite-derived immunomodulators) might increase risk of infection-related malignancy.

METHODS

Ethics Statement. All procedures with animals were carried out according to the recommendations of the national guidelines for animal caring: 12.08.1977 N 755 "On measures to further improve the organizational forms of work using experimental animals" and approved by the Siberian State Medical University (license number 5786 issued on February 26, 2018).

Parasites, Experimental Opisthorchiasis Model, and Experimental Design. Twenty golden Syrian hamsters (*Mesocricetus auratus*) of both genders were purchased from the animal facility of the Institute of Bioorganic Chemistry Academicians M. M. Shemyakin and U. A. Ovchinnikov. The hamsters were housed in groups of five with food and water provided ad libitum for the duration of the experiment. After 1 week of acclimatization, at the age of 6 weeks old, 10 animals (5 males and 5 females) were infected orally with 50 *O. felineus* metacercariae in phosphate-buffered saline (PBS) (infected group). *O. felineus* metacercariae were obtained from naturally infected fish captured from the Ob river in endemic areas of Tomsk, Russian Federation. The viable metacercariae were collected and identified by microscopy from the pepsin-HCl-digested muscular and subcutaneous tissues. The remaining 10 hamsters (5 males and 5 females) were subjected to the same procedures with PBS (control group). During the experiment, one female animal of the infected group died.

https://doi.org/10.1021/acsinfecdis.1c00026
ACS Infect. Dis. 2021, 7, 906−916

Sample Collection and Assessment of the Infection. Blood serum, urine, and feces samples were collected in the 20th week postinfection from the animals of both groups. The hamsters were placed individually into sterile empty glass crates for collecting urine and feces, where separation of stool from urine was facilitated. The urine samples were collected into labeled cryotubes over ice and stored frozen at −80 °C. Two to three pellets of animal feces were collected into labeled cryotubes over ice and stored frozen at −80 °C until NMR analysis.

On the day after collecting the biofluid samples, the animals were sacrificed, and tissue samples and serum were collected for NMR and morphological analysis. The blood samples were collected into vacutainer tubes (no additive), left on ice for coagulation, and centrifugated at 3500*g* for 10 min. The provided serum was transferred into cryotubes and stored at −80 °C. Small samples of the three intestinal parts (colon, jejunum, and ileum), part of the liver, and the right kidney were transferred into 5 mL tubes containing a solution of 4% buffered formalin for subsequent histological analysis via hematoxylin and eosin staining. The left kidney and the spleen were harvested and transferred into a 2 mL cryotube, immediately immersed in liquid nitrogen, and stored at −80 °C for NMR analysis. Small portions (∼0.5 cm) of intestinal tissue (colon, jejunum, and ileum) were cut from the middle of each section. Then, the intestinal tissue portions were washed with PBS, transferred into cryotubes, immersed in liquid nitrogen, and stored at −80 °C for NMR analysis. The rest of the liver from infected animals after collecting histological material was treated over ice to remove flukes from the bile ducts. The liver then was collected into the cryotubes, immersed in liquid nitrogen, and stored at −80 °C. The liver from control group of animals was treated by the same procedure as the liver of infected animals.

Assessment of the infection intensity was performed by counting worms in the liver and bile ducts for each infected hamster.

Sample Preparation for NMR Data Acquisition. All chemicals used for the buffer solutions were purchased from Sigma-Aldrich except for the ^2H_2O (Cortecnet) and the 3-(trimethylsilyl)propionic-2,2,3,3-d_4 acid sodium salt (TSP) (Cambridge Isotope Laboratories Inc.). Two buffer solutions were prepared. Buffer solution A was a disodium phosphate buffer in H_2O/D_2O (80/20) with pH of 7.4 containing 6.15 mM NaN_3 and 4.64 mM TSP. Buffer solution B was a disodium phosphate buffer in D_2O (pH = 7.4) containing 1.5 M K_2HPO_4, 2 mM NaN_3, and 4 mM TSP. The 96-well Ritter Deepwell plates were acquired from Novaveth B.V., and NMR tubes were purchased from Bruker Biospin Ltd.

The serum samples were thawed at 4 °C and were mixed by inverting the tubes 10 times. Next, the samples (120 μL) were mixed with 120 μL of buffer solution A using a Gilson 215 liquid handler in combination with a Bruker SampleTrack system. For each sample, 190 μL of buffer−serum mixture was transferred into 3 mm SampleJet NMR tubes in 96-tube racks using a modified Gilson 215 tube filling station and kept at 6 °C on a SampleJet sample changer while queued for acquisition.

The sample preparation of urine samples was performed using the method as described elsewhere[8] with minor changes in the sample preparation step: 630 μL of urine from each sample was mixed with 70 μL of buffer solution B; 565 μL of urine−buffer mixture was transferred to 5 mm SampleJet NMR tubes.

Two to three fecal pellets from each animal were weighed and mixed with Milli-Q water at a ratio of 1:5. The mixtures were homogenized by bead beating with zirconium oxide beads of 1 mm diameter for 3 min in a Bullet Blender 24 system (Next Advance Inc., USA). The homogenized mixtures were centrifuged at 16 100*g* for 20 min at 4 °C. The supernatants were carefully collected, and centrifugation was repeated under the same conditions. After the second centrifugation, 500 μL of supernatant of each sample was taken for filtration.

The filters used for the filtration step were molecular weight cutoff (MWCO) filters Vivaspin 500 3 kDa (GE Healthcare, UK). These filters need to be carefully washed prior to use in order to remove the significant glycerol contamination that was present in the unused filters. The washing procedure was as follows: the filters were centrifuged twice with 0.5 mL of Milli-Q water at 15 000*g* for 20 min at 20 °C. Every time residual water was removed from the filters by allowing it to drain out properly. Eppendorf tubes were filled with 1 mL of Milli-Q water, after which the rinsed filters were inserted. A volume of 0.5 mL of Milli-Q water was added into the filter, and the Eppendorf tubes were stored overnight at 4 °C. Then water was removed by centrifugation at 15 000*g* for 20 min at 20 °C, the filters were rinsed again under the same conditions, and then residual water was removed from a filter by letting it drain. The filters were used immediately to avoid destroying of the membrane.

Using the washed filters, the supernatant of the second centrifugation of the feces−water mixture was then filtrated at 15 000*g* for 20 min at 20 °C four times. Subsequently 150 μL of filtrate was mixed with 30 μL of Milli-Q water and 20 μL of buffer solution B. Then 190 μL of the mixture of each sample was transferred into 3 mm SampleJet NMR tubes.

The frozen liver, the spleen, the left kidney, and samples of the three parts of the intestine (colon, jejunum, and ileum) were weighed and mixed with a 70% methanol/30% Milli-Q water mixture with the tissue/solvent ratio = 1:3. The mixtures were homogenized by applying six cycles of 1 min of bead beating and 1 min cooling on ice. For bead beating, zirconium oxide beads of 1 mm diameter were used. The homogenized mixtures were centrifuged at 16 100*g* for 20 min at 4 °C. The supernatants were collected and dried under a stream of nitrogen. Then, the dry residues were resuspended with D_2O and then centrifugated at 16 100*g* for 10 min at 4 °C. Buffer B was added to the supernatant for a final buffer concentration of 10%. The sample/buffer mixtures of liver, kidney, spleen, jejunum, and ileum were transferred into 3 mm SampleJet NMR tubes, and colon samples were transferred into 1.7 mm SampleJet NMR tubes.

NMR Data Acquisition and Spectral Data Processing. ^1H NMR data were collected using a Bruker 600 MHz AVANCE II spectrometer equipped with a 5 mm TCI cryogenic probe head and a z-gradient system. A Bruker SampleJet sample changer was used for sample insertion and removal. Two NMR protocols were used, one for the serum samples and one for all the others.

All experiments were recorded at 300 K, except the serum samples, which were recorded at 310 K. A fresh sample of 99.8% methanol-d_4 was used for temperature calibration.[29] The axial shims were optimized automatically before every measurement. Durations of 90° pulses were automatically

https://doi.org/10.1021/acsinfecdis.1c00026
ACS Infect. Dis. 2021, 7, 906−916

calibrated for each individual sample using a homonuclear-gated mutation experiment[30] on the locked and shimmed samples after automatic tuning and matching of the probe head.

Four NMR experiments were performed on each serum sample: 1D NOESY, CPMG, diffusion edited, and 2D JRES. The NOESY1D experiment was recorded using the first increment of a NOESY pulse sequence[31] with presaturation (γB_1 = 25 Hz) during a relaxation delay of 4 s and a mixing time of 10 ms for efficient water suppression.[32] Sixty four scans of 65 ,536 points covering a sweep width of 18 029 Hz were recorded and zero-filled to 65 536 complex points prior to Fourier transformation. A standard 1D Carr−Purcell−Meiboom−Gill (CPMG) pulse sequence with presaturation was used to for the acquisition of T_2-filtered spectra. A pulse train of 128 refocusing pulses with individual spin echo delays of 0.6 ms was applied resulting in a total T_2 filtering delay of 78 ms. After applying four dummy scans, a total of 73 728 data points covering a spectral width of 12 019 Hz were collected. Otherwise, the parameters were similar to the 1D NOESY experiment. The diffusion-edited spectrum was recorded with presaturation. The pulse sequence parameters were similar to those of the 1D NOESY experiment. An exponential window function was applied with a line-broadening factor of 1.0 Hz. After Fourier transformation, the spectra were automatically phase and baseline corrected and automatically referenced to the internal standard (TSP = 0.0 ppm). Afterward, the spectra were referenced to the anomeric glucose doublet (5.23 ppm).

J-resolved spectra (JRES) were recorded with a relaxation delay of 2 s with presaturation (γB_1 = 25 Hz) and eight scans for each increment in the indirect dimension. A data matrix of 40 × 12 288 data points was collected covering a sweep width of 78 × 10 000 Hz. A sine-shaped window function was applied to both dimensions and the data was zero-filled to 256 × 16 384 complex data points prior to Fourier transformation. In order to remove the skew, the resulting data matrix was tilted along the rows by shifting each row (k) by 0.4992·(128-k) points and symmetrized about the central horizontal lines.

The NMR parameters were similar as for serum, except for the use of a stronger presaturation field (γB_1 = 50 Hz). For the 1D experiments, 16 scans of 65 536 points covering a sweep width of 12 336 Hz were accumulated, except for the colon and ileum samples, where 64 scans were used. Other parameters were similar as to those of the serum 1D NOESY experiments. The 2D JRES experiments were also recorded with similar settings as to those of serum, with two scans per increment in the indirect dimension, and eight scans per increment for colon and ileum.

Identification and Quantification of the Metabolites. Identification of small metabolites (<1000 Da) was performed by an exhaustive search of the total 1D and 2D JRES data using the proprietary Bbiorefcode (Bruker Biospin Ltd.).

Quantification of the small metabolites and glycogen in liver samples was performed manually with the Chenomx NMR suite 8.1 software (Chenomx Inc.). Concentrations were extracted using the known TSP concentration (0.4 mM).

Serum lipoproteins and cholesterol were identified and quantified as described elsewhere.[9]

GS-MS Analysis of Serum Fatty Acids. GC-MS analysis of medium- and long-chain fatty acids in serum samples was performed accordingly the protocol.[33] GC-MS analysis of serum short-chain fatty acids was performed accordingly the protocol.[34]

Data Analysis. All data analyses were performed with the R statistical environment (http://www.r-project.org/, R versions 3.6.0, 3.6.1). Basic data table handling was performed with a help of the *tidyverse* package (version 1.1.2); the *data.Normalization* function of the clusterSim (version 0.48-1) package was used for the data normalization before the modeling. For the evaluation of the principle source of variance on multiblock data and selection of the most relevant data blocks, the Multi-Omics Factor Analysis (MOFA) package 1.2.0 and mixKernel (version 0.3) were used. To dissect an optimal subset of metabolites, we used a regression approach, namely, the DIABLO (Data Integration Analysis for Biomarker discovery using Latent variable approaches for 'Omics studies) tool of the mixOmics package (version 6.10.1). DIABLO combines a surprised multiblock modeling with variable selection. K-means clustering was computed using the standard of R command. For data visualization the ggplot2 package (version 3.2.1) was used.

Metabolic network enrichment analysis was performed in the MetExplore v2.23.15 environment, using the KEGG global network for a Chinese hamster (*Cricetulus griseus*) (a network for a golden Syrian hamster (*Mesocricetus auratus*) is not available currently).[35,36] The metabolites selected by the multiblock regression modeling were used for the pathway enrichment on each block separately. Only the pathways with $p < 0.05$ after Bonferroni correction were included in the resulting graphs.

■ ASSOCIATED CONTENT

Supporting Information

The Supporting Information is available free of charge at https://pubs.acs.org/doi/10.1021/acsinfecdis.1c00026.

Table with quantified metabolites for all data blocks used in the manuscripts, representative histological images, additional descriptive and statistical material (PDF)

NMR data (XLSX)

■ AUTHOR INFORMATION

Corresponding Author

Oleg A. Mayboroda − *Center for Proteomics and Metabolomics, Leiden University Medical Center, Leiden 2333ZA, The Netherlands;* orcid.org/0000-0001-8739-9875; Email: o.a.mayboroda@lumc.nl

Authors

Daria Kokova − *Department of Parasitology, Leiden University Medical Center, Leiden 2333ZA, The Netherlands; Laboratory of Clinical Metabolomics, Tomsk State University, Tomsk 634050, Russian Federation*

Aswin Verhoeven − *Center for Proteomics and Metabolomics, Leiden University Medical Center, Leiden 2333ZA, The Netherlands*

Ekaterina A. Perina − *Central Research Laboratory Siberian State Medical University, Tomsk 634050, Russian Federation*

Vladimir V. Ivanov − *Central Research Laboratory Siberian State Medical University, Tomsk 634050, Russian Federation*

Marieke Heijink − *Center for Proteomics and Metabolomics, Leiden University Medical Center, Leiden 2333ZA, The Netherlands*

Maria Yazdanbakhsh − *Department of Parasitology, Leiden University Medical Center, Leiden 2333ZA, The Netherlands*

Complete contact information is available at: https://pubs.acs.org/10.1021/acsinfecdis.1c00026

Notes

The authors declare no competing financial interest.

■ ACKNOWLEDGMENTS

The research was supported by The Tomsk State University competitiveness improvement programme.

■ REFERENCES

(1) Keiser, J., and Utzinger, J. (2005) Emerging Foodborne Trematodiasis. *Emerging Infect. Dis.*, 1507−1514.
(2) Petney, T. N., Andrews, R. H., Saijuntha, W., Wenz-Mücke, A., and Sithithaworn, P. (2013) The Zoonotic, Fish-Borne Liver Flukes Clonorchis Sinensis, Opisthorchis Felineus and Opisthorchis Viverrini. *Int. J. Parasitol.*, 1031−1046.
(3) Mairiang, E., and Mairiang, P. (2003) *Acta Trop. 88*, 221−227.
(4) Pungpak, S., Chalermrut, K., Harinasuta, T., Viravan, C., Schelp, P. F., Hempfling, A., Schlattmann, P., and Bunnag, D. (1994) Opisthorchis Viverrini Infection in Thailand: Symptoms and Signs of Infection-a Population-Based Study. *Trans. R. Soc. Trop. Med. Hyg. 88* (5), 561−564.
(5) Wang, A., Luan, H. H., and Medzhitov, R. (2019) An Evolutionary Perspective on Immunometabolism. *Science. 363*, eaar3932.
(6) Kokova, D., and Mayboroda, O. A. (2019) Twenty Years on: Metabolomics in Helminth Research. *Trends Parasitol. 35*, 282−288.
(7) Singer, B. H., Utzinger, J., Ryff, C. D., Wang, Y., and Holmes, E. (2007) Exploiting the Potential of Metabonomics in Large Population Studies: Three Venues. In *The Handbook of Metabonomics and Metabolomics*, pp 289−325, Chapter 11, Elsevier.
(8) Kokova, D. A., Kostidis, S., Morello, J., Dementeva, N., Perina, E. A., Ivanov, V. V., Ogorodova, L. M., Sazonov, A. E., Saltykova, I. V., and Mayboroda, O. A. (2017) Exploratory Metabolomics Study of the Experimental Opisthorchiasis in a Laboratory Animal Model (Golden Hamster, Mesocricetus Auratus). *PLoS Negl. Trop. Dis. 11* (10), e0006044.
(9) Kokova, D., Verhoeven, A., Perina, E. A., Ivanov, V. V., Knyazeva, E. M., Saltykova, I. V., and Mayboroda, O. A. (2020) Plasma Metabolomics of the Time Resolved Response to Opisthorchis Felineus Infection in an Animal Model (Golden Hamster, Mesocricetus Auratus). *PLoS Negl. Trop. Dis. 14* (1), e0008015.
(10) Li, J. V., Holmes, E., Saric, J., Keiser, J., Dirnhofer, S., Utzinger, J., and Wang, Y. (2009) Metabolic Profiling of a Schistosoma Mansoni Infection in Mouse Tissues Using Magic Angle Spinning-Nuclear Magnetic Resonance Spectroscopy. *Int. J. Parasitol. 39* (5), 547−558.
(11) Buffet, P. A., Safeukui, I., Deplaine, G., Brousse, V., Prendki, V., Thellier, M., Turner, G. D., and Mercereau-Puijalon, O. (2011) The Pathogenesis of Plasmodium Falciparum Malaria in Humans: Insights from Splenic Physiology. *Blood 117*, 381−392.
(12) Boonpucknavig, S., Boonpucknavig, V., Tanvanich, S., Doungchawee, G., and Thamavit, W. (1992) Development of Immune-Complex Glomerulonephritis and Amyloidosis in Syrian Golden Hamsters Infected with Opisthorchis Viverrini. *J. Med. Assoc. Thailand 75* (Suppl 1), 7−19.
(13) Lapteva, G. F. (1990) Opistorkhoznaia Nefropatiia. *Vrac. delo Kiev* No. 2, 67−69.
(14) Mariette, J., and Villa-Vialaneix, N. (2018) Unsupervised Multiple Kernel Learning for Heterogeneous Data Integration. *Bioinformatics 34* (6), 1009−1015.
(15) Argelaguet, R., Velten, B., Arnol, D., Dietrich, S., Zenz, T., Marioni, J. C., Buettner, F., Huber, W., and Stegle, O. (2018) Multi-Omics Factor Analysis—a Framework for Unsupervised Integration of Multi-omics Data Sets. *Mol. Syst. Biol. 14* (6), e8124.
(16) Newsholme, E. A., Newsholme, P., and Curi, R. (1987) The Role of the Citric Acid in Cells of the Immune System and Its Importance in Sepsis, Trauma and Burns. *Biochem. Soc. Symp.*, 145−162.
(17) Ahola-Olli, A. V., Mustelin, L., Kalimeri, M., Kettunen, J., Jokelainen, J., Auvinen, J., Puukka, K., Havulinna, A. S., Lehtimäki, T., Kähönen, M., Juonala, M., Keinänen-Kiukaanniemi, S., Salomaa, V., Perola, M., Järvelin, M. R., Ala-Korpela, M., Raitakari, O., and Würtz, P. (2019) Circulating Metabolites and the Risk of Type 2 Diabetes: A Prospective Study of 11,896 Young Adults from Four Finnish Cohorts. *Diabetologia 62* (12), 2298−2309.
(18) Wu, J. H. Y., Marklund, M., Imamura, F., Tintle, N., Ardisson Korat, A. V., de Goede, J., Zhou, X., Yang, W. S., de Oliveira Otto, M. C., Kröger, J., Qureshi, W., Virtanen, J. K., Bassett, J. K., Frazier-Wood, A. C., Lankinen, M., Murphy, R. A., Rajaobelina, K., Del Gobbo, L. C., Forouhi, N. G., Luben, R., Khaw, K. T., Wareham, N., Kalsbeek, A., Veenstra, J., Luo, J., Hu, F. B., Lin, H. J., Siscovick, D. S., Boeing, H., Chen, T. A., Steffen, B., Steffen, L. M., Hodge, A., Eriksdottir, G., Smith, A. V., Gudnason, V., Harris, T. B., Brouwer, I. A., Berr, C., Helmer, C., Samieri, C., Laakso, M., Tsai, M. Y., Giles, G. G., Nurmi, T., Wagenknecht, L., Schulze, M. B., Lemaitre, R. N., Chien, K. L., Soedamah-Muthu, S. S., Geleijnse, J. M., Sun, Q., Harris, W. S., Lind, L., Ärnlöv, J., Riserus, U., Micha, R., and Mozaffarian, D. (2017) Omega-6 Fatty Acid Biomarkers and Incident Type 2 Diabetes: Pooled Analysis of Individual-Level Data for 39 740 Adults from 20 Prospective Cohort Studies. *Lancet Diabetes Endocrinol. 5* (12), 965−974.
(19) Meikle, P. J., Wong, G., Barlow, C. K., Weir, J. M., Greeve, M. A., MacIntosh, G. L., Almasy, L., Comuzzie, A. G., Mahaney, M. C., Kowalczyk, A., Haviv, I., Grantham, N., Magliano, D. J., Jowett, J. B. M., Zimmet, P., Curran, J. E., Blangero, J., and Shaw, J. (2013) Plasma Lipid Profiling Shows Similar Associations with Prediabetes and Type 2 Diabetes. *PLoS One 8* (9), No. e74341.
(20) Pfeuffer, M., and Jaudszus, A. (2016) Pentadecanoic and Heptadecanoic Acids: Multifaceted Odd-Chain Fatty Acids. *Adv. Nutr. 7* (4), 730−734.
(21) Jenkins, B. J., Seyssel, K., Chiu, S., Pan, P. H., Lin, S. Y., Stanley, E., Ament, Z., West, J. A., Summerhill, K., Griffin, J. L., Vetter, W., Autio, K. J., Hiltunen, K., Hazebrouck, S., Stepankova, R., Chen, C. J., Alligier, M., Laville, M., Moore, M., Kraft, G., Cherrington, A., King, S., Krauss, R. M., De Schryver, E., Van Veldhoven, P. P., Ronis, M., and Koulman, A. (2017) Odd Chain Fatty Acids; New Insights of the Relationship between the Gut Microbiota, Dietary Intake, Biosynthesis and Glucose Intolerance. *Sci. Rep. 7* (1), 44845.
(22) Guasch-Ferré, M., Hruby, A., Toledo, E., Clish, C. B., Martínez-González, M. A., Salas-Salvadó, J., and Hu, F. B. (2016) Metabolomics in Prediabetes and Diabetes: A Systematic Review and Meta-Analysis. *Diabetes Care 39*, 833−846.
(23) Wiria, A. E., Sartono, E., Supali, T., and Yazdanbakhsh, M. (2014) Helminth Infections, Type-2 Immune Response, and Metabolic Syndrome. *PLoS Pathog. 10* (7), No. e1004140.
(24) Fedorova, O. S., Kovshirina, Y. V., Kovshirina, A. E., Fedotova, M. M., Deev, I. A., Petrovskiy, F. I., Filimonov, A. V., Dmitrieva, A. I., Kudyakov, L. A., Saltykova, I. V., Odermatt, P., and Ogorodova, L. M. (2017) Opisthorchis Felineus Infection and Cholangiocarcinoma in the Russian Federation: A Review of Medical Statistics. *Parasitol. Int. 66* (4), 365−371.
(25) Hall, J. C., Heel, K., and McCauley, R. (1996) Glutamine. *Br. J. Surg.*, 305−312.
(26) Sripa, B. (2003) Pathobiology of Opisthorchiasis: An Update. *Acta Trop. 88*, 209−220.
(27) Ren, M., Zhang, S. H., Zeng, X. F., Liu, H., and Qiao, S. Y. (2015) Branched-Chain Amino Acids Are Beneficial to Maintain Growth Performance and Intestinal Immune-Related Function in Weaned Piglets Fed Protein Restricted Diet. *Asian-Australas. J. Anim. Sci. 28* (12), 1742−1750.
(28) Powell, J. D., Pollizzi, K. N., Heikamp, E. B., and Horton, M. R. (2012) Regulation of Immune Responses by MTOR. *Annu. Rev. Immunol. 30*, 39−68.

(29) Findeisen, M., Brand, T., and Berger, S. (2007) A 1H-NMR Thermometer Suitable for Cryoprobes. *Magn. Reson. Chem. 45* (2), 175−178.
(30) Wu, P. S. C., and Otting, G. (2005) Rapid Pulse Length Determination in High-Resolution NMR. *J. Magn. Reson. 176* (1), 115−119.
(31) Kumar, A., Ernst, R. R., and Wüthrich, K. (1980) A Two-Dimensional Nuclear Overhauser Enhancement (2D NOE) Experiment for the Elucidation of Complete Proton-Proton Cross-Relaxation Networks in Biological Macromolecules. *Top. Catal. 95* (1), 1−6.
(32) Price, W. S. (1999) Water Signal Suppression in NMR Spectroscopy. *Annu. Rep. NMR Spectrosc. 38* (C), 289−354.
(33) Hoving, L. R., Heijink, M., van Harmelen, V., van Dijk, K. W., and Giera, M. (2018) GC-MS Analysis of Medium- and Long-Chain Fatty Acids in Blood Samples. *Methods Mol. Biol. 1730*, 257−265.
(34) Hoving, L. R., Heijink, M., van Harmelen, V., van Dijk, K. W., and Giera, M. (2018) GC-MS Analysis of Short-Chain Fatty Acids in Feces, Cecum Content, and Blood Samples. *Methods Mol. Biol. 1730*, 247−256.
(35) Chazalviel, M., Frainay, C., Poupin, N., Vinson, F., Merlet, B., Gloaguen, Y., Cottret, L., and Jourdan, F. (2018) MetExploreViz: Web Component for Interactive Metabolic Network Visualization. *Bioinformatics 34* (2), 312−313.
(36) Kanehisa, M. (2002) *The KEGG Database* (Bock, G., and Goode, J. A., Eds.), Novartis Foundation Symposia, pp 91−103, Vol. *247*, John Wiley & Sons, Ltd..

https://doi.org/10.1021/acsinfecdis.1c00026
ACS Infect. Dis. 2021, 7, 906−916